

# Impact of a Spinning Supermassive Black Hole on the Orbit and Gravitational Waves of a Nearby Compact Binary

YUN FANG,<sup>1,2</sup> XIAN CHEN,<sup>3,4</sup> AND QING-GUO HUANG<sup>1,2</sup>

<sup>1</sup>*CAS Key Laboratory of Theoretical Physics, Institute of Theoretical Physics, Chinese Academy of Sciences, Beijing 100190, China*

<sup>2</sup>*School of Physical Sciences, University of Chinese Academy of Sciences, No. 19A Yuquan Road, Beijing 100049, China*

<sup>3</sup>*Astronomy Department, School of Physics, Peking University, Beijing 100871, China*

<sup>4</sup>*Kavli Institute for Astronomy and Astrophysics at Peking University, Beijing 100871, China*

(Dated: August 6, 2019; Received; Revised; Accepted; Published)

## ABSTRACT

Recent theoretical studies suggest that stellar-mass binary black holes (BBHs) would merge more efficiently due to the Kozai-Lidov mechanism if these binaries form in the vicinity of supermassive black holes (SMBHs). Since SMBHs are likely rotating rapidly, we continue our earlier study on the generalization of the Kozai-Lidov formalism to include the spin of the SMBH and study the evolution of a nearby BBH. We find that the eccentricity and orbital inclination of the BBH is significantly affected, because the spin (i) forces the orbital plane of the center-of-mass of the BBH around the SMBH to precess (the Lense-Thirring effect) and (ii) imposes an additional gravitomagnetic force on the BBH. As a result, the merger time of the BBH could be significantly different. We calculate the waveform from the BBH in one representative example and study its detectability by a milli-Hertz GW detector, such as the Laser Interferometer Space Antenna (LISA). We find that the signal is distinguishable from that in the case without spin. Our results imply that the BBHs in the LISA band could potentially be used to probe the spin of the SMBHs in galaxy centers.

*Keywords:* gravitational waves – methods: data analysis – celestial mechanics – galaxies: nuclei

## 1. INTRODUCTION

The Laser Interferometer Gravitational-wave Observatory (LIGO) and the Virgo detectors have detected ten binary black hole (BBH) mergers and one binary neutron star inspiraling event during the first two observing runs (Abbott et al. 2016d,c, 2017a,b,c, 2016b, 2017d, 2018). The origin of the LIGO/Virgo BBHs is unclear. In the conventional picture, BBHs form either in massive binary stars or star clusters (Abbott et al. 2016a). Recent studies, however, suggest that the centers of galaxies (Miller & Lauburg 2009), especially those hosting supermassive black holes (SMBHs), are also important places for BBH formation (e.g. Antonini & Perets 2012). In these environments, the merger rate of BBHs could be enhanced (see e.g. Chen et al. 2019, and references therein). The causes of this enhance-

ment include a high escape velocity for compact objects, a large concentration of black holes (BHs) due to the “mass segregation effect”, a tidal perturbation of the BBHs by the SMBHs, and a hydrodynamical friction on each BH if gas is present. The resulting merger rate could be a significant fraction of the LIGO/Virgo event rate according to recent calculations (Hong & Lee 2015; VanLandingham et al. 2016; Hoang et al. 2018; Petrovich & Antonini 2017; Arca-Sedda & Gualandris 2018; Fragione et al. 2018; Bartos et al. 2017; Stone et al. 2017; Mckernan et al. 2018).

According to these previous theoretical studies, a small fraction of BBHs could either form at (Inayoshi et al. 2017; Stone et al. 2017; Bartos et al. 2017; Mckernan et al. 2018; Secunda et al. 2019) or be captured to places very close to the SMBHs (e.g. Addison et al. 2015; Chen & Han 2018). As a result, a triple system, composed of a BBH (as the “inner binary”) revolving around an SMBH (as the “outer binary”), could form. Because of the perturbation by the SMBH, the inner BBH would undergo a “Kozai-Lidov oscillation”, during which the internal eccentricity of the BBH can be

fangyun@itp.ac.cn

xian.chen@pku.edu.cn

huangqg@itp.ac.cn

excited to a large value (Kozai 1962; Lidov 1962; Naoz 2016). The consequence is a faster merger of the BBH (Antonini & Perets 2012) or an early detection of the BBH by a space-borne detector (such as the Laser Interferometer Space Antenna, LISA) when the semi-major axis of the binary is still large (Meiron et al. 2017; Hoang et al. 2019; Randall & Xianyu 2019).

General relativistic effects are important during the evolution of the triple. It has been shown that relativistic precession could suppress the Kozai-Lidov (K-L) evolution, and that gravitational wave (GW) radiation could circularize and limit the maximum eccentricity of the inner binary (Wen 2003; Antonini & Perets 2012; Seto 2013; VanLandingham et al. 2016; Fragione & Leigh 2018; Chen & Han 2018; Hoang et al. 2019; Zhang et al. 2019). However, these previous works normally assume a Schwarzschild metric for the central SMBH. In reality, SMBHs are spinning (e.g. Reynolds 2014, 2013; Akiyama et al. 2019a,b). The spin would induce a “gravitomagnetic field” (Nichols et al. 2011) in the spacetime, which causes an additional precession to the outer orbit known as the “Lense-Thirring effect”. This precession will invalidate the standard assumption in the K-L formalism that the angular momentum of the outer orbit is effectively unchanged (Will 2017). Moreover, the gravitomagnetic force also affects the inner binary orbit, which is not included in the K-L formalism either.

Recently, we have extended the K-L formalism to include the spin effects and found a modulation of the K-L cycle on a relatively long timescale (Fang & Huang 2019). Here we apply our method to study in more detail the evolution of a stellar-mass BBH around a rotating SMBH. We pay special attention to the GWs emitted by the inner binary and look for imprint of the spin.

The paper is organized as follows. In Section 2, we calculate the dynamical evolution of a BBH around a spinning SMBH using our extended K-L formulae including post-Newtonian (PN) corrections. More specifically, we include pericenter precession (1PN), radiation reaction (2.5PN), and the most importantly, the effects of spin acting on the orbits (1.5PN). We refer to this model as “K-L+1PN+RR+Spin” and compare the results with that from the model without spin, which we denote as “K-L+1PN+RR”. In Section 3, as an example, we calculate the waveform of a BBH around a SMBH similar to that in our Galactic Center. We show in Section 4 that in principle the results with and without spin are distinguishable by LISA. Finally, we summarize our findings in Section 5.

## 2. THE DYNAMICAL EVOLUTION

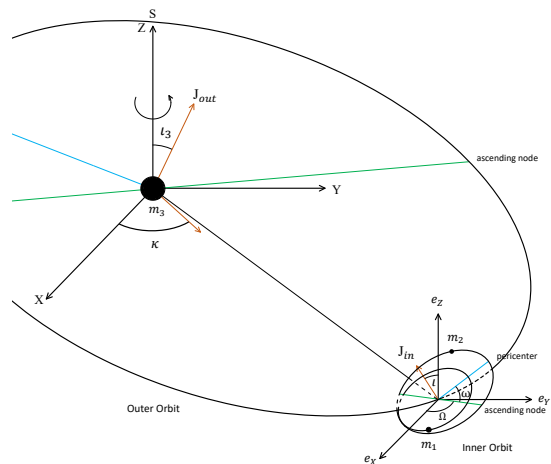


**Figure 1.** Configuration of our triple system seen from a fixed reference frame of  $(X, Y, Z)$  with basis vectors  $(\mathbf{e}_X, \mathbf{e}_Y, \mathbf{e}_Z)$ . The vectors  $\mathbf{J}_{\text{out}}$  and  $\mathbf{J}_{\text{in}}$  are, respectively, the angular momenta of the outer and inner binary. Moreover,  $\iota_3$  and  $\iota$  are the inclination angles of the outer and inner orbits,  $\kappa$  is the angle between the projection of  $\mathbf{J}_{\text{out}}$  in the  $(X, Y)$  plane and  $\mathbf{e}_X$ ,  $\Omega$  is the longitude of the ascending node of the inner orbit, and  $\omega$  the pericenter angle.

The configuration of our triple system is illustrated in Figure 1. Here,  $m_1, m_2$  are the masses of the two BHs of the inner binary, which is revolving around a SMBH with mass  $m_3$ . The orbital parameters are defined in a fixed coordinate system of  $(X, Y, Z)$ , with the  $Z$ -axis aligned with the spin of the SMBH. Moreover,  $\mathbf{J}_{\text{out}}$  and  $\mathbf{J}_{\text{in}}$  are, respectively, the angular momenta of the outer and inner binaries. The main consequence of a rotating SMBH is to induce a gravitomagnetic field in which a moving particle will feel a Lorentz-like force perpendicular to its velocity (e.g. Thorne & Hartle 1984; Nichols et al. 2011; Poisson & Will 2014). This gravitomagnetic force affects both the outer and inner orbits (Fang & Huang 2019). For the outer orbit, the net effect is a Lense-Thirring precession of its angular momentum, which changes the angle  $\kappa$  or, equivalently, changes the longitude of the ascending node. For the inner orbit, the gravitomagnetic force modulates the inclination ( $\iota$ ), ascending node ( $\Omega$ ), and pericenter ( $\omega$ ), and in this way alters the K-L oscillation. These effects are not present in the K-L formalism based on non-spinning SMBHs.

To illustrate the effects of the spin on the K-L oscillation, we show two representative cases. In both examples, we set  $m_1 = 20M_\odot$ ,  $m_2 = 10M_\odot$ , and  $m_3 = 4 \times 10^6 M_\odot$ , presenting the SMBH population similar to the one in the Galactic Center. We also choose a spin value of  $a = 0.9m_3$  for the central SMBH, where we have assumed  $G = c = 1$ . The semi-major axis of the BBH is chosen to be  $\alpha = 0.031$  AU, and that for the

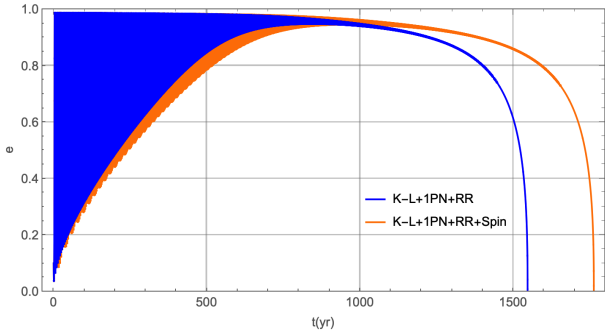


**Figure 2.** Evolution of the eccentricity of the BBH in our first example. The orange curve is computed using our model including the spin effects, while the blue one is computed without spin.

outer orbit is  $\mathcal{A} = 30$  AU. The corresponding eccentricities are, respectively,  $e = 0.1$  and  $E = 0.1$ . We choose these parameters so that the BBH and the SMBH form a stable triple system, meanwhile the BBH is close enough to the SMBH to be affected by its spin.

In the first example, we use  $\iota_3 = 60^\circ$ ,  $\iota = 70^\circ$ ,  $\omega = 20^\circ$ ,  $\Omega = 100^\circ$ , and  $\Omega_3 = 0$  as the initial conditions, where  $\Omega_3$  is the longitude of ascending node of the outer orbit. The resulting K-L oscillation is shown in Figure 2. The orange curve refers to the “K-L+1PN+RR+Spin” model where the spin effects are included, and the blue one refers to the “K-L+1PN+RR” model where the SMBH has zero spin. We can see that the eccentricity oscillates between  $e = 0.1$  and  $e \simeq 1$  at the beginning of the evolution. This is a result of the K-L mechanism. The oscillation amplitude decreases with time because the suppression of the K-L cycle by the 1PN precession becomes stronger as the semi-major axis decreases due to GW radiation. After about  $10^3$  years the eccentricity no longer oscillates because GW radiation starts to dominate the evolution of the BBH. In this example, the merger time of the BBH is longer when spin is included.

In the second example, we change the initial angles to  $\iota = 140^\circ$ ,  $\omega = 10^\circ$ ,  $\Omega = 60^\circ$ , and keep the other parameters the same. The results are shown in Figure 3. In this case, the presence of the spin shortens the lifetime of the BBH.

From the above two examples, we find that the spin affects the lifetime of the BBH significantly, by about 14% to 25% relative to the lifetime around a non-spinning SMBH. This difference could affect the event rate of BBH mergers around SMBHs. We plan to study the impact on the LIGO/Virgo/LISA observations in a future work.

Here, we are interested in calculating the GWs generated by the inner binary. Since the waveform is closely related to the projection of the two stellar BHs in the

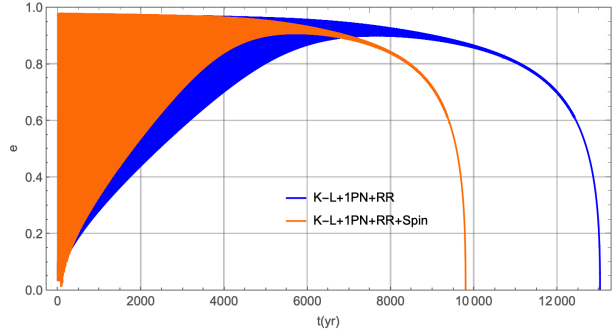


**Figure 3.** The same as Figure 2 but for different angles in the initial conditions.

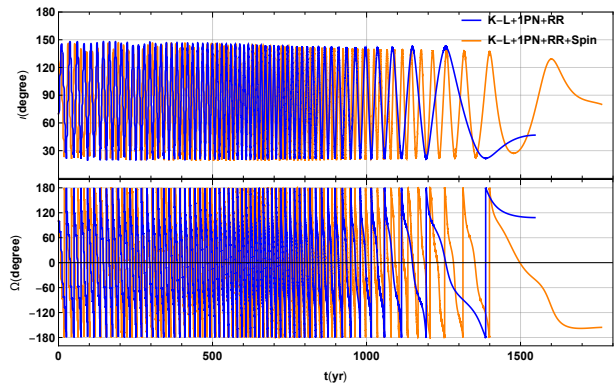


**Figure 4.** Evolution of  $\iota$  and  $\Omega$ . The line styles are the same as in Figure 2.

plane perpendicular to the line-of-sight, we proceed to study the orientation of the orbital plane (depending on  $\iota$  and  $\Omega$ ) and the direction of the pericenter (depending on  $\iota$ ,  $\Omega$ , and  $\omega$ ) of the inner orbit. The results corresponding to our first example are shown in Figures 4 and 5. We can see that  $\iota$  oscillates more frequently and  $\Omega$  precesses faster when spin is added. By the end of our simulation, the BBH coalesces with completely different  $\iota$  and  $\Omega$  compared to the case without spin. As for  $\omega$ , the precession is slower when spin is included. The cause is that in the first example the semi-major axis  $a$  shrinks more slowly when spin is present.

The spin of the SMBH also affects the outer orbit by inducing a Lense-Thirring precession. As can be seen in the lower panel of Figure 6, the consequence is a precession of the angular momentum of the outer binary about the axis of the spin. We note that the longitude of the ascending node (the aforementioned  $\Omega_3$ ) is equal to  $\kappa + \pi/2$ , and hence we do not plot it here. In the classic picture of the Lense-Thirring effect, the inclination of the orbit ( $\iota_3$ ) is a constant. However, the upper panel of Figure 6 shows that  $\iota_3$  oscillates, although the amplitude is small. The oscillation is caused by the coupling of the inner and outer orbits in the K-L mechanism.

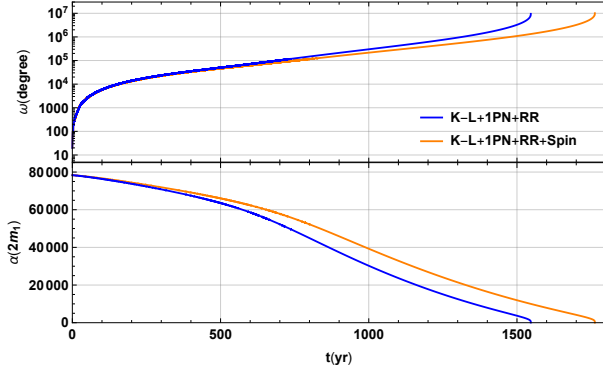


**Figure 5.** Evolution of  $\omega$  and  $\alpha$ , and the line styles are the same as in Figure 2.

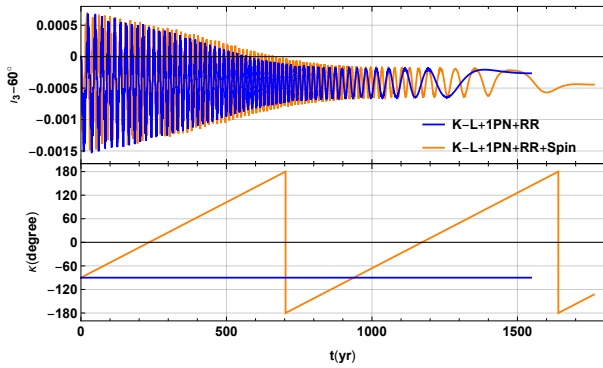


**Figure 6.** The same as Figure 4 but for  $\kappa$  and  $l_3$ .

The precession of the  $\Omega_3$  angle of the outer orbit, in turn, affects the dynamical evolution of the inner one. This is because  $(\Omega - \Omega_3)$  and  $l_3$  enter the equations of motion of the inner binary (Fang & Huang 2019). In addition, the spin has a direct impact on the evolution of  $l$ ,  $\omega$ , and  $\Omega$ . The combined effect causes a different evolution of the inner binary in our “K- L+1PN+RR+Spin” model.

Moreover, the longitude of pericenter of the outer orbit also precesses due to the spin. However, it is decoupled from the evolution of the other orbital elements, in the sense that it does not enter the equations of motion of the other orbital elements (see e.g. Naoz 2016; Will 2017; Fang & Huang 2019), and hence we could ignore it here. Only from the octuple order does this angle couple with the other orbital elements (see e.g. Naoz et al. 2013; Naoz 2016), but the coupling is small in our example because the ratio of the two semi-major axis,  $\alpha/A$ , is small.

### 3. CALCULATION OF THE WAVEFORM

Now we use the angles derived in the last section to calculate the GW waveform from the inner binary. To

facilitate the calculation, we assume that the source is at a distance of  $r$  from the detector, the sky location is  $(\theta, \varphi)$ , and the polarization angle is  $\psi$  (see Apostolatos et al. 1994, for the definition of the angles). We further denote  $(\gamma, \beta)$  as the angles describing the orientation of the wave vector in the source frame  $(x, y, z)$ , which is defined in such a way that the  $(x, y)$  plane aligns with the orbital plane of the BBH, the  $x$ -axis is in the direction of the pericenter, and the  $z$ -axis aligns with  $\mathbf{J}_{\text{in}}$ . In this way, the  $(x, y, z)$  frame is linked to the  $(X, Y, Z)$  coordinate system by a Euler transformation with the angles  $(\omega, l, \Omega)$ . To calculate  $(\gamma, \beta)$ , we fix the line-of-sight along the  $X$ -axis, for simplicity. As a result, we have

$$\cos \gamma = \mathbf{e}_z \cdot \mathbf{e}_X = \sin l \sin \Omega, \quad (1)$$

$$\begin{aligned} \sin \gamma &= \frac{(\mathbf{e}_X - (\mathbf{e}_z \cdot \mathbf{e}_X)\mathbf{e}_z) \cdot \mathbf{e}_Y}{|\mathbf{e}_X - (\mathbf{e}_z \cdot \mathbf{e}_X)\mathbf{e}_z|} \\ &= \frac{2 - 2 \sin^2 l \sin^2 \Omega}{\sqrt{2 \cos 2l \sin^2 \Omega + \cos 2\Omega + 3}}, \end{aligned} \quad (2)$$

and

$$\cos \beta = \frac{2 \cos \omega \cos \Omega - 2 \cos l \sin \omega \sin \Omega}{\sqrt{2 \cos 2l \sin^2 \Omega + \cos 2\Omega + 3}}, \quad (3)$$

$$\sin \beta = -\frac{2 \cos l \cos \omega \sin \Omega + 2 \sin \omega \cos \Omega}{\sqrt{2 \cos 2l \sin^2 \Omega + \cos 2\Omega + 3}} \quad (4)$$

(see also Eq. (11) in Fang & Huang 2019).

The strains of the  $+$  and  $\times$  polarizations of the GWs can now be calculated with

$$h_+ = \frac{1}{2}(\gamma^j \gamma^k - \beta^j \beta^k) h_{jk}^{\text{TT}}, \quad (5)$$

$$h_\times = \frac{1}{2}(\gamma^j \beta^k + \beta^j \gamma^k) h_{jk}^{\text{TT}}, \quad (6)$$

where  $\boldsymbol{\gamma} := (\cos \gamma \cos \beta, \cos \gamma \sin \beta, -\sin \gamma)$  and  $\boldsymbol{\beta} := (-\sin \beta, \cos \beta, 0)$ . Here,  $h_{jk}^{\text{TT}}$  is the TT projection of the GW strain  $h_{jk}$ . The GW waveform of an eccentric orbit is composed of many Fourier modes (see e.g. Maggiore 2007), and the  $n$ -th mode can be calculated with

$$\begin{aligned} h_{+,n} &= -\frac{\pi^2 f^2 \mu n^2}{r} \{2C_n \sin 2\beta (\cos 2\gamma + 3) \sin(2\pi n f t) \\ &\quad + \cos(2\pi n f t) [(A_n - B_n) \cos 2\beta (\cos 2\gamma + 3) \\ &\quad - 2(A_n + B_n) \sin^2 \gamma]\}, \end{aligned} \quad (7)$$

$$\begin{aligned} h_{\times,n} &= -\frac{4\pi^2 f^2 \mu n^2 \cos \gamma}{r} [(B_n - A_n) \sin 2\beta \cos(2\pi n f t) \\ &\quad + 2C_n \cos 2\beta \sin(2\pi n f t)], \end{aligned} \quad (8)$$

$$(9)$$

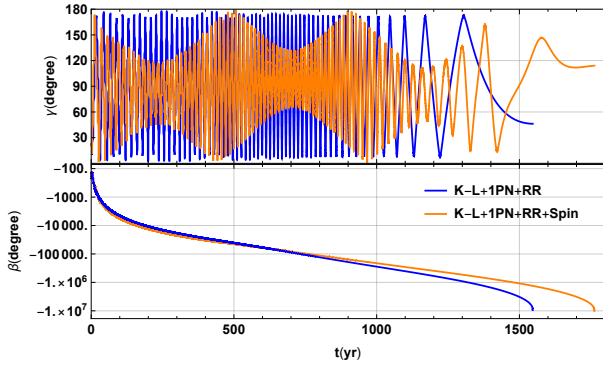


**Figure 7.** Evolution of  $\gamma$  (upper panel) and  $\beta$  (lower panel). The blue curves correspond to the model without spin and the orange ones with spin.

where  $f$  is the radial orbital frequency of the inner binary,  $\mu = m_1 m_2 / (m_1 + m_2)$  is the reduced mass, and

$$A_n = \frac{\alpha^2}{n} [J_{n-2}(ne) - J_{n+2}(ne) - 2eJ_{n-1}(ne) + 2eJ_{n+1}(ne)], \quad (10)$$

$$B_n = -\frac{(1-e^2)\alpha^2}{n} [J_{n-2}(ne) - J_{n+2}(ne)], \quad (11)$$

$$C_n = \frac{\sqrt{1-e^2}\alpha^2}{n} [J_{n-2}(ne) + J_{n+2}(ne) - eJ_{n-1}(ne) - eJ_{n+1}(ne)], \quad (12)$$

$$(13)$$

We can see that the waveform is closely related to the angles  $\gamma$  and  $\beta$ . Figure 7 shows the difference of  $\gamma$  and  $\beta$  in our first example. We find that in this example,  $\gamma$  changes in two ways when spin is included. First, it oscillates with a higher frequency. Second, its amplitude shows a periodic modulation. The first effect is caused by a combination of the Lense-Thirring effect on the outer orbit and the gravitomagnetic force acting on the inner orbit. The latter effect, i.e., the periodic modulation of the amplitude, is closely related to the Lense-Thirring precession of the outer orbit, since the timescale is the same as the precession of  $\kappa$  shown in Figure 6. The behavior of  $\beta$  is similar to  $\omega$  in Figure 5. The difference is mainly a minus symbol because in the source frame the direction of the precession reverses.

We note that the revolution of the BBH around the SMBH, in principle, also generates GWs (e.g. see an example in Chen & Han 2018). We do not calculate them because for the parameters considered in this work the corresponding frequency is much lower than mHz, and hence outside the LISA band. Moreover, the revolution should also periodically modulate the phase of the GWs (from the BBH), as a consequence of the Doppler frequency shift (Inayoshi et al. 2017; Meiron et al. 2017),

as well as modulate the amplitude due to the Lorentz transformation of the wave vectors (Torres-Orjuela et al. 2018). We do not include these effects in our calculations because in our examples they are of PN order; they are secondary effects relative to the modulation of  $\gamma$  and  $\beta$ .

## 4. MATCHED FILTERING

### 4.1. General consideration

Now we study whether or not LISA could detect the spin of the SMBH from the waveform of the BBH. We take the first example in Section 2 for illustrative purposes because, as we will show below, the BBH evolves into the LISA band on a relative short timescale. It is known that a highly eccentric BBH emits a broad spectrum of GWs (Peters & Mathews 1963). The peak of this spectrum is located at a frequency closely linked to the pericenter distance  $\alpha(1-e)$ , i.e.,

$$f_{\text{peak}} = \frac{\sqrt{m_1 + m_2}(1+e)^{-0.3046}}{\pi [\alpha(1-e)]^{3/2}} \quad (14)$$

(Wen 2003). If this peak enters the LISA band ( $10^{-3}$  –  $10^{-1}$  Hz), the BBH could be detected. Figure 8 shows the evolution of  $f_{\text{peak}}$  in our first example. We find that the BBH dwells in the LISA band during the first 1500–1700 years of the evolution. Afterwards, the BBH moves into the LIGO/Virgo band and coalesces.

To see more details of the K-L evolution during a period comparable to the observational timescale, we shown in Figure 9 the evolution of  $\alpha$ ,  $e$ ,  $\gamma$ , and  $\beta$  during the first 12 years. We find that the K-L timescale is about four years and it becomes shorter when spin of the SMBH is introduced. This result indicates that (i) LISA could detect the entire K-L cycle if the observational period is longer than four years and (ii) the difference of

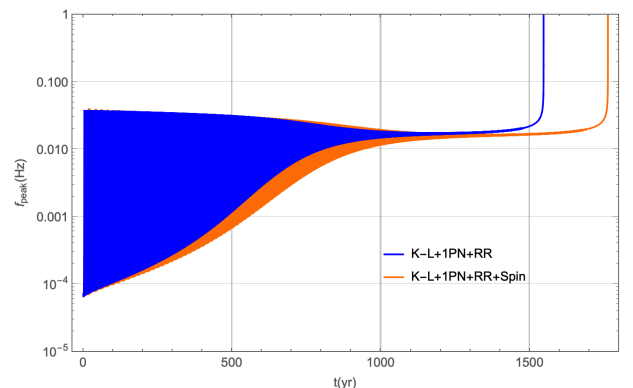


**Figure 8.** Evolution of the peak frequency of the GWs from the inner BBH. The line styles and the model parameters are the same as in Figure 2.

the waveform induced by the spin of the SMBH could be detectable by LISA.

In practice, LISA employs a method called the “matched filtering” to discern the difference between two waveforms (Finn 1992; Cutler & Flanagan 1994; Lindblom et al. 2008). For example, given  $h_1$  and  $h_2$ , the inner product is defined as

$$\langle h_1 | h_2 \rangle = 2 \int_0^\infty \frac{\tilde{h}_1^*(f) \tilde{h}_2(f) + \tilde{h}_1(f) \tilde{h}_2^*(f)}{S_h(f)} df, \quad (15)$$

where  $S_h(f)$  is the spectral noise density (Eq. (1) in Robson et al. 2019) and  $\tilde{h}_i(f)$  denotes the Fourier transformation

$$\tilde{h}(f) = \int_{-\infty}^\infty e^{2\pi i f t} h(t) dt. \quad (16)$$

The two waveforms are indistinguishable if the condition

$$\langle \delta h | \delta h \rangle = \langle h_1 - h_2 | h_1 - h_2 \rangle < 1 \quad (17)$$

is satisfied.

In real observations, we are often in a situation where  $h_1 \simeq h_2$ . In this case, the calculation of Equation (17) can be significantly simplified. One can, instead, calculate a quantity called the “fitting factor” (FF) (Apostolatos et al. 1994; Lindblom et al. 2008), defined as

$$\text{FF} = \frac{\langle h_1 | h_2 \rangle}{\sqrt{\langle h_1 | h_1 \rangle \langle h_2 | h_2 \rangle}}, \quad (18)$$

and compare it with a threshold FF defined as

$$\text{FFS} = 1 - \frac{1}{\langle h_1 | h_1 \rangle + \langle h_2 | h_2 \rangle}. \quad (19)$$

The latter FFS is closely related to the signal-to-noise ratio (SNR), i.e.,  $\text{SNR} = \sqrt{\langle h | h \rangle}$ . If  $h_1 \simeq h_2$ , we have  $\text{FFS} \simeq 1 - 1/(2 \text{SNR}^2)$ , and the criterion of Equation (17) is equivalent to  $\text{FF} > \text{FFS}$ . For example, LISA will claim a detection as soon as SNR becomes 10. This means for LISA sources, FFS is at least 0.995, and only the waveform template with  $\text{FF} > 0.995$  is an acceptable match to the signal.

To account for high eccentricities, the inner product defined in Equation (15) can be computed using the harmonics of  $h_1$  and  $h_2$ , i.e.,

$$\langle h_1 | h_2 \rangle = 2 \sum_{n=1}^\infty \frac{\tilde{h}_{1,n}^*(f_n) \tilde{h}_{2,n}(f_n) + \tilde{h}_{1,n}(f_n) \tilde{h}_{2,n}^*(f_n)}{S_h(f_n)} df_n. \quad (20)$$

We calculate the frequency of the  $n$ -th harmonic with the approximation  $f_n \simeq n f_0$ , where  $f_0$  is the radial orbital frequency. It is an approximation because we have neglected the shift of the GW frequency caused by the

precession of the pericenter. The approximation is acceptable here because the shift of  $f_n$  is  $\dot{\omega}/\pi$  (Barack & Cutler 2004), which is of PN order and is much smaller than  $f_0$ .

#### 4.2. Specific implementation

In our own problem, the difference between  $h_1$  and  $h_2$  is caused by the spin of the SMBH. For the convenience of the following analysis, we denote the waveform calculated from the “K-L+1PN+RR” model as  $h_1(e_1, \alpha_1, \gamma_1, \beta_1)$  and that from the “K-L+1PN+RR+Spin” as  $h_2(e_2, \alpha_2, \gamma_2, \beta_2)$ . Each waveform is a weighted sum of the two polarizations defined in Section 3, i.e.,

$$h(t) = F_+(\theta, \varphi, \psi) \frac{\sqrt{3}}{2} h_+(t, r, e, \gamma, \beta) + F_\times(\theta, \varphi, \psi) \frac{\sqrt{3}}{2} h_\times(t, r, e, \gamma, \beta), \quad (21)$$

where  $F_+$  and  $F_\times$  are the “antenna patterns”. The coefficient  $\sqrt{3}/2$  comes from the fact that the actual angle between LISA arms is  $60^\circ$  (Berti et al. 2005; Nishizawa et al. 2016). For simplicity, we average the source location angles ( $\theta$  and  $\varphi$ ) and the polarization angle ( $\psi$ ), so that we do not need to consider the motion of the LISA arms (also see Barack & Cutler 2004; Robson et al. 2019). As a result of the average, we have  $\langle F_+^2 \rangle = \langle F_\times^2 \rangle = 1/5$  and  $\langle F_+ F_\times \rangle = 0$  (Flanagan & Hughes 1998; Robson et al. 2019).

We notice that in this example, the radial orbital frequency of the BBH in the first four years (the first K-L cycle) of evolution is almost a constant. Therefore, for each Fourier mode  $S_h(f_n)$  is also a constant. In this case, by Parseval’s theorem, the integration in the frequency domain can be performed in the time domain (Barack & Cutler 2004),

$$\begin{aligned} \langle h_1 | h_2 \rangle &= 2 \sum_{n=1}^\infty \frac{1}{S_h(f_n)} \int_0^{\Delta t} |h_{1,n}(t) h_{2,n}(t)| dt \quad (22) \\ &= \sum_{n=1}^\infty \frac{3/10}{S_h(f_n)} \int_0^{\Delta t} (|h_{1+,n} h_{2+,n}| + |h_{1\times,n} h_{2\times,n}|) dt, \quad (23) \end{aligned}$$

where we have applied the result  $\langle F_+ F_\times \rangle = 0$  derived above so that the cross terms with  $h_{1+,n} h_{2\times,n}$  and  $h_{1\times,n} h_{2+,n}$  vanish. Moreover, the results for  $|h_{+,n}|^2 + |h_{\times,n}|^2$  and  $|h_{1+,n} h_{2+,n}| + |h_{1\times,n} h_{2\times,n}|$  do not depend on the definition of the GW polarizations in Equation 5 and 6 as long as we averaged out  $F_+$  and  $F_\times$  (Poisson & Will 2014). By averaging  $|h_{+,n}|^2 + |h_{\times,n}|^2$  and  $|h_{1+,n} h_{2+,n}| + |h_{1\times,n} h_{2\times,n}|$  over GW phase, we have (fol-

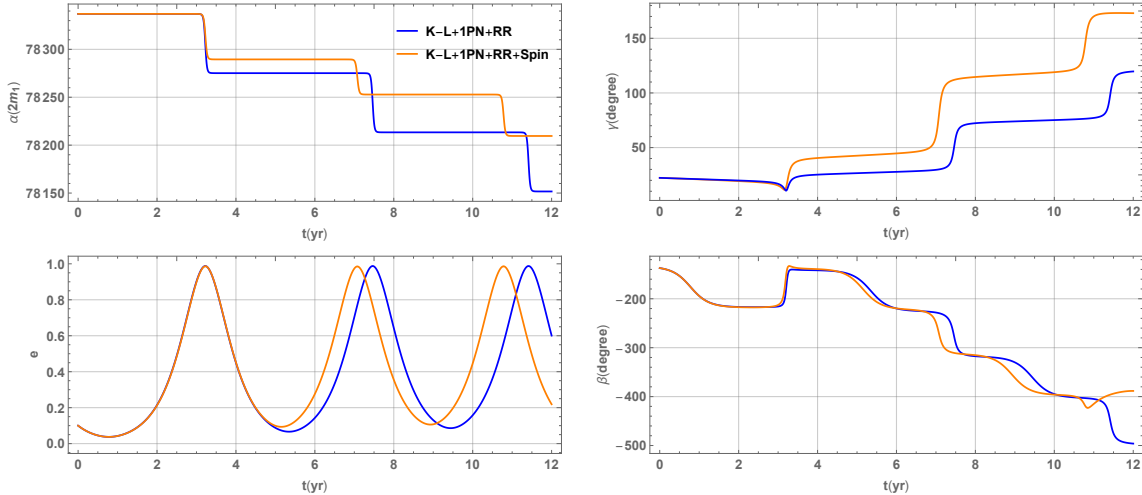


**Figure 9.** Evolution of  $e, \alpha, \gamma, \beta$  in the first 12 years for our first example. The unit of  $\alpha$  is  $2m_1$ , i.e., the Schwarzschild radius of the more massive BH in the binary.

lowing [Maggiore 2007](#))

$$|h_{1+,n}|^2 + |h_{1\times,n}|^2 = \frac{\pi^4 f^4 \mu^2 n^4}{2r^2} (4C_{1n}^2 \sin^2 2\beta_1 (\cos 2\gamma_1 + 3)^2 + ((A_{1n} - B_{1n}) \cos 2\beta_1 (\cos 2\gamma_1 + 3) - 2(A_{1n} + B_{1n}) \sin^2 \gamma_1)^2 + 16 \cos^2 \gamma_1 ((A_{1n} - B_{1n})^2 \sin^2 2\beta_1 + 4C_{1n}^2 \cos^2 2\beta_1)), \quad (24)$$

$$|h_{2+,n}|^2 + |h_{2\times,n}|^2 = (|h_{1+,n}|^2 + |h_{1\times,n}|^2)(1 \rightarrow 2), \quad (25)$$

$$|h_{1+,n} h_{2+,n}| + |h_{1\times,n} h_{2\times,n}| = \frac{\pi^4 f^4 \mu^2 n^4}{2r^2} (16 \cos \gamma_1 \cos \gamma_2 (4 \cos 2\beta_1 \cos 2\beta_2 C_{1n} C_{2n} + \sin 2\beta_1 \sin 2\beta_2 (A_{1n} - B_{1n})(A_{2n} - B_{2n})) + (\cos 2\beta_1 (\cos 2\gamma_1 + 3)(A_{1n} - B_{1n}) - 2 \sin^2 \gamma_1 (A_{1n} + B_{1n})) \times (\cos 2\beta_2 (\cos 2\gamma_2 + 3)(A_{2n} - B_{2n}) - 2 \sin^2 \gamma_2 (A_{2n} + B_{2n})) + 4 \sin 2\beta_1 \sin 2\beta_2 (\cos 2\gamma_1 + 3)(\cos 2\gamma_2 + 3) C_{1n} C_{2n}), \quad (26)$$

With the above preparations, we can proceed to calculate the FF defined in Equation (18). Assuming that our source is in the Galactic Center, at a distance of  $r = 8$  kpc, and LISA observes it for four years, we find for our first example that  $\text{FF} = 0.834$  and  $\text{FFS} = 0.999997$ . The result  $\text{FF} < \text{FFS}$  indicates that if there is such a BBH around the SMBH in the Galactic Center, LISA should be able to detect the effects induced by the spin.

## 5. CONCLUSIONS

In this paper we have studied the impact of the spin of a supermassive black hole (SMBH) on the orbital evolution of a nearby compact binary. Our model is based on our previous theoretical work on the extension of the Kozai-Lidov formalism to include the effects due to the

spin of the tertiary body ([Fang & Huang 2019](#)). By comparing the orbital evolution of the BBH in the cases with and without the spin effects, we find the following results from our representative examples. (i) When the spin is present, the dynamical evolution of the BBH is significantly different, mainly caused by the Lense-Thirring precession of the outer orbit and the gravitomagnetic force acting on the inner orbit. (ii) The merger time of the BBH could be elongated or shortened by the presence of the spin, depending on the initial orbital angles. (iii) The combined effects of the Lense-Thirring precession (of the outer binary) and the gravitomagnetic force (on the inner binary) causes the inclination ( $\gamma$ ) of the inner orbit relative to the line-of-sight to oscillate more rapidly, while the Lense-Thirring precession also periodically modulates the amplitude of the oscillation of  $\gamma$  on the same timescale.

We have also developed an analytical framework to calculate the GWs from the BBHs in our problem and used it to study the impact of the spin on LISA waveforms. We find the following differences from our representative example. (i) The polarization angle (azimuth angle  $\beta$ ) of the waveform precesses differently when spin is included in our calculation. (ii) The period of the Kozai-Lidov oscillation, and hence the timescale on which the BBH enters and exits the LISA band, changes as a result of the spin of the SMBH. (iii) Given the triple in our representative example, we find that  $\text{FF} < \text{FFS}$  when the SNR of the source is high enough, which indicates that for such sources LISA should be able to detect the effects induced by the spin of the SMBH. Because the evolution of the inner BBH depends on the initial conditions, in a future work we will conduct a thorough survey of the parameter space and identify those triple

systems where the effects of the spin of the SMBHs are detectable by LISA.

This work is supported by the NSFC grants No. 11690021, 11575271, 11747601, 11873022. QGH acknowledges support by the Strategic Priority Research

Program of the Chinese Academy of Sciences (Grant No. XDB23000000, XDA15020701), and the Top-Notch Young Talents Program of China. XC is partly supported by the Strategic Priority Research Program of the Chinese Academy of Sciences through the grants No. XDB23040100 and XDB23010200.

## REFERENCES

- Abbott, B. P., et al. 2016a, *ApJ*, 818, L22
- . 2016b, *PhRvX*, 6, 041015, [Erratum: *PhRvX* 8,no.3,039903(2018)]
- . 2016c, *PhRvL*, 116, 241103
- . 2016d, *PhRvL*, 116, 061102
- . 2017a, *PhRvL*, 118, 221101, [Erratum: *PhRvL* 121,no.12,129901(2018)]
- . 2017b, *ApJ*, 851, L35
- . 2017c, *PhRvL*, 119, 141101
- . 2017d, *PhRvL*, 119, 161101
- . 2018, arXiv:1811.12907
- Addison, E., Laguna, P., & Larson, S. 2015
- Akiyama, K., et al. 2019a, *ApJ*, 875, L1
- . 2019b, *ApJ*, 875, L4
- Antonini, F., & Perets, H. B. 2012, *ApJ*, 757, 27
- Apostolatos, T. A., Cutler, C., Sussman, G. J., & Thorne, K. S. 1994, *PhRvD*, 49, 6274
- Arca-Sedda, M., & Gualandris, A. 2018, *MNRAS*, 477, 4423
- Barack, L., & Cutler, C. 2004, *PhRvD*, 69, 082005
- Bartos, I., Kocsis, B., Haiman, Z., & Macquettark, S. 2017, *ApJ*, 835, 165
- Berti, E., Buonanno, A., & Will, C. M. 2005, *PhRvD*, 71, 084025
- Chen, X., & Han, W.-B. 2018, *CmPhy.*, 1, 53
- Chen, X., Li, S., & Cao, Z. 2019, *MNRAS*, 485, L141
- Cutler, C., & Flanagan, E. E. 1994, *PhRvD*, 49, 2658
- Fang, Y., & Huang, Q.-G. 2019, *PhRvD*, 99, 103005
- Finn, L. S. 1992, *PhRvD*, 46, 5236
- Flanagan, E. E., & Hughes, S. A. 1998, *PhRvD*, 57, 4535
- Fragione, G., Grishin, E., Leigh, N. W. C., Perets, H., & Perna, R. 2018
- Fragione, G., & Leigh, N. 2018, *MNRAS*, 480, 5160
- Hoang, B.-M., Naoz, S., Kocsis, B., Farr, W., & McIver, J. 2019, *ApJ*, 875, L31
- Hoang, B.-M., Naoz, S., Kocsis, B., Rasio, F. A., & Dosopoulou, F. 2018, *ApJ*, 856, 140
- Hong, J., & Lee, H. M. 2015, *MNRAS*, 448, 754
- Inayoshi, K., Tamanini, N., Caprini, C., & Haiman, Z. 2017, *PhRvD*, 96, 063014
- Kozai, Y. 1962, *Astron. J.*, 67, 591
- Lidov, M. L. 1962, *Planetary and Space Science.*, 9, 719
- Lindblom, L., Owen, B. J., & Brown, D. A. 2008, *PhRvD*, 78, 124020
- Maggiore, M. 2007, *Gravitational Waves* (Oxford: Oxford Univ. Press)
- Mckernan, B., et al. 2018, *ApJ*, 866, 66
- Meiron, Y., Kocsis, B., & Loeb, A. 2017, *ApJ*, 834, 200
- Miller, M. C., & Lauburg, V. M. 2009, *ApJ*, 692, 917
- Naoz, S. 2016, *ARA&A*, 54, 441
- Naoz, S., Farr, W. M., Lithwick, Y., Rasio, F. A., & Teyssandier, J. 2013, *MNRAS*, 431, 2155
- Nichols, D. A., et al. 2011, *PhRvD*, 84, 124014
- Nishizawa, A., Berti, E., Klein, A., & Sesana, A. 2016, *PhRvD*, 94, 064020
- Peters, P. C., & Mathews, J. 1963, *PhRvD*, 131, 435
- Petrovich, C., & Antonini, F. 2017, *ApJ*, 846, 146
- Poisson, E., & Will, C. M. 2014, *Gravity: Newtonian, Post-Newtonian, Relativistic* (Cambridge: Cambridge Univ. Press)
- Randall, L., & Xianyu, Z.-Z. 2019, arXiv:1902.08604
- Reynolds, C. S. 2013, *CQGra*, 30, 244004
- . 2014, *Space Sci. Rev.*, 183, 277
- Robson, T., Cornish, N. J., & Liug, C. 2019, *CQGra*, 36, 105011
- Secunda, A., Bellovary, J., Mac Low, M.-M., et al. 2019, *ApJ*, 878, 85
- Seto, N. 2013, *PhRvL*, 111, 061106
- Stone, N. C., Metzger, B. D., & Haiman, Z. 2017, *MNRAS*, 464, 946
- Thorne, K. S., & Hartle, J. B. 1984, *PhRvD*, 31, 1815
- Torres-Orjuela, A., Chen, X., Cao, Z., Amaro-Seoane, P., & Peng, P. 2018, arXiv e-prints, arXiv:1806.09857
- VanLandingham, J. H., Miller, M. C., Hamilton, D. P., & Richardson, D. C. 2016, *ApJ*, 828, 77
- Wen, L. 2003, *ApJ*, 598, 419
- Will, C. M. 2017, *PhRvD*, 96, 023017
- Zhang, F., Shao, L., & Zhu, W. 2019, *ApJ*, 877, 87